Journal of
Mechanics of
Materials and Structures

MORPHOLOGICAL PROCESSING OF PROPER ORTHOGONAL MODES FOR CRACK DETECTION IN BEAM STRUCTURES

Konstantinos C. Gryllias, Ioannis N. Koukoulis, Christos T. Yiakopoulos, Ioannis A. Antoniadis and Christopher G. Provatidis

Volume 4, Nº 6 June 2009

mathematical sciences publishers

JOURNAL OF MECHANICS OF MATERIALS AND STRUCTURES
Vol. 4, No. 6, 2009

MORPHOLOGICAL PROCESSING OF PROPER ORTHOGONAL MODES FOR CRACK DETECTION IN BEAM STRUCTURES

KONSTANTINOS C. GRYLLIAS, IOANNIS N. KOUKOULIS, CHRISTOS T. YIAKOPOULOS, IOANNIS A. ANTONIADIS AND CHRISTOPHER G. PROVATIDIS

A two-step approach for crack detection in beam structures is presented. As a first step, a number of proper orthogonal modes (POMs) of a beam are extracted, using proper orthogonal decomposition, a powerful and elegant method (closely related to principal component analysis) aimed at obtaining low-dimensional approximations of high-dimensional processes, taking into account nonlinearities and minimizing noise effects.

Then, alternatively to other approaches, morphological processing is proposed for the further processing of the POMs. The basic concept of morphological processing is to modify the shape of an object by transforming it through its interaction with another object, called the structuring element. Using an appropriate morphological processing procedure, the position and the depth of the cracks can be estimated by isolating the sudden local change effect of the cracks on the spatial variation of the shape of each POM. For this purpose, the four basic morphological operators (dilation, erosion, opening, closing) are compared, using two different types of structuring elements. The erosion operator with a spline structuring element is shown to present the best results.

Finally, the performance of the method is assessed on different beam structures affected by breathing cracks, with respect to the influence of several factors, such as boundary conditions, crack location, crack depth, crack distance, measurement noise level and space resolution of measurement points. In all cases, the method presents a robust behavior.

1. Introduction

The presence of cracks in engineering structures, especially in aerospace, civil and mechanical engineering infrastructures, may lead to catastrophic failures with serious results (loss of lives, extensive downtimes, delays, etc). As a consequence, a plethora of analytical, numerical and experimental methodologies, approaches and techniques have been proposed for crack detection, focused on different types of structures including aircraft, civil infrastructures such as bridges and buildings, as well as laboratory specimens, such as beams and plates. Such work is reviewed, for example, in [Sohn et al. 2004; Doebling et al. 1998; Dimarogonas 1996; Randall 2002].

Damage can be defined by comparing different responses of a system, as they result from changes into its state, introduced as a result of the damage [Sohn et al. 2004]. A five-step damage state classification system was proposed in [Rytter 1993], examining the existence, location, type and extent of the damage, and lastly the possibility of a prognosis for the remaining useful life of the system. The presence of a crack in a structure introduces local flexibility and as a result, provokes changes at the dynamic behavior

Keywords: vibration analysis, crack detection, proper orthogonal decomposition, morphological processing.

of the structure. Therefore, a large number of methodologies for crack detection have been developed, based on detecting changes in various dynamic properties of the structure, such as natural frequencies, modal damping, mode shapes, transfer functions etc., as those changes result as a consequence of the damage.

The easiest, simplest and most popular method for damage detection is by identifying changes in natural frequencies. In a relevant pioneer paper [Lifshitz and Rotem 1969], the use of vibration measurements for damage detection is proposed. A methodology for damage detection, localization and quantification based on natural frequency shifts is proposed in [Cawley and Adams 1979]. In order to overcome difficulties related to natural-frequency-shifts-based crack detection, methodologies utilizing changes in mode shapes have been also proposed. A very interesting comparison between a frequency-based and a mode shape-based method for damage detection in beam like structures is presented in [Kim et al. 2003]. Changes in mode shapes are much more sensitive, compared to changes in natural frequencies. However, a crack may not influence the lower mode shapes, which are usually measured. Operational and environmental conditions, such as temperature, humidity, loads and boundary conditions may cause changes that hide those resulting from damage [Farrar et al. 1994; Cawley 1997].

In case of multiple cracks, additional issues are involved, such as orientation of cracks with respect to each other, change in mode shapes and complexity. In [Ostachowicz and Krawczuk 1991] the effect of positions and depths of two cracks on the natural frequency of cantilever beams is analyzed. The effect of crack depth and location on the eigenfrequencies of a double-cracked beam is studied in [Ruotolo and Surace 1997]. Among others, some very good reviews on analysis of structures under multiple cracks are presented in [Ruotolo and Surace 1997; Sekhar 2008].

Most of these works concerning cracks include a combination of analytical or computational models with experimental results [Alvandi and Cremona 2006; Wang and Deng 1999; Bamnios et al. 2002; Chang and Chen 2005; Douka et al. 2003; Loutridis et al. 2004; Hadjileontiadis et al. 2005a; Sahin and Shenoi 2003]. Among them [Alvandi and Cremona 2006] and [Sahin and Shenoi 2003] involve finite element models. As a result of the advanced capabilities of modelling methods such as FEM, substitution of the experimental procedure by appropriate FEM based computations and random noise addition has been proposed to simulate the experimental procedure [Luzzato 2003; Andreaus et al. 2007; Zhong and Oyadiji 2007; Galvanetto and Violaris 2007]. Additionally, in order to lead to a more reliable analysis, the practice of adding artificial noise to the analytical or numerical results has been also used [Alvandi and Cremona 2006; Hadjileontiadis et al. 2005b].

Concerning analytical models, as those are used particularly in beams with open cracks, the region of the crack was initially modelled as an area characterized by a reduced flexural rigidity [Rytter 1993], while later, the beam was simulated considering the area of the crack as a rotational spring [Wang and Deng 1999], [Bamnios et al. 2002; Chang and Chen 2005; Douka et al. 2003; Loutridis et al. 2004; Hadjileontiadis et al. 2005a; Hadjileontiadis et al. 2005b]. Additionally, an analytical model has been proposed [Douka et al. 2004] to model a plate with a transverse crack. However, considering the most appropriate modelling approach for a crack in a structure such as a beam, the presence of a crack causes the structure to exhibit a strongly nonlinear behavior, if the crack successively opens and closes ("breathes")@during the vibration. In order to take into account a breathing crack, beam models with bilinear spring-mass system have been developed [Luzzato 2003; Cheng et al. 1999; Loutridis et al. 2005; Douka and Hadjileontiadis 2005; Guo and Billings 2007]. These models mostly assume that the crack

is either open or closed; however there is at least one implementation of a continuous breathing crack model [Cheng et al. 1999]. Concerning the spectral effect of a breathing crack, it is generally considered [Luzzato 2003; Cheng et al. 1999] that the use of the breathing crack model is necessary, because in this case the natural frequency reduction is much smaller than that for an open crack case.

In this paper, an alternative approach for crack detection in structures is presented. As a first step, the proper orthogonal decomposition (POD) method is used, in order to obtain a number of the proper orthogonal modes (POMs) of a cracked cantilever beam. POD, closely related to principal component analysis, is a powerful and elegant method of data analysis aimed at obtaining low-dimensional approximate descriptions of high-dimensional nonlinear processes and eliminating noise effects [Lumley 1967; Azeez and Vakakis 1997; Lenaerts et al. 2001].

Then, alternatively to other approaches, morphological processing is proposed in this paper for analyzing the shape of the resulting POMs. The basic concept of morphological processing [Serra 1982; Maragos and Schafer 1987] is to modify the shape of an object, equivalently considered as a set, by transforming it through its interaction with another object, called the "structuring element". Using appropriate morphological processing, the position of the crack can be estimated by isolating the local sudden change effect of the crack on the spatial variation of each POM.

The rest of the paper is organized as follows. The method of proper orthogonal decomposition of structures is reviewed in Section 2 and the basic concepts of morphological processing of one-dimensional functions are reviewed in Section 3. A sensitivity analysis is performed is Section 4 between a 3D, a plain stress 2D and a plain strain 2D finite element modeling approach for a cantilever beam and as a result, the 2D plane stress model is shown to present the optimal behavior, providing the same actual level of accuracy with far less needed computational time. The four basic morphological operators (dilation, erosion, opening, closing) using two different types of structuring elements are compared in Section 5 and the erosion operator with a spline structuring element is shown to present the best results. Finally, the performance of the method is assessed on a cantilever beam in Section 6 and on a simple beam in Section 7, with respect to the influence of several factors, such as crack location, crack depth, crack distance, measurement noise level and space resolution of measurement points. In all cases, the method presents a robust behavior with respect to the determination of both the location and the depth of the crack.

2. Proper orthogonal decomposition (POD)

Proper orthogonal decomposition (POD) was first applied to turbulence problems by [Lumley 1967]. It identifies a useful set of basis functions and the dimension of the subspace necessary to achieve a satisfactory approximation of the system. It has been shown [Feeny 1997] that the application of POD to measured displacements of a discrete structure with a known mass matrix can lead to an estimation of the normal modes. The POD also facilitates the resolution of the partial differential equations through their projection into a reduced-order model [Azeez and Vakakis 1997] and for this reason it has been applied for vibro-impact systems.

2.1. ***Mathematical formulation of the POD.*** The POMs are shown here to be the eigenfunctions of the space correlation tensor. The definitions and formulation presented here follow closely the ones used in [Lenaerts et al. 2001]. Let $u(x, t)$ be a random field on some domain Ω. Since the POD requires dealing

with zero-mean signals, it is necessary to define $v(x,t)$ by subtracting the mean $U(x) = \langle u \rangle$ from $v(x,t)$:

$$u(x,t) = U(x) + v(x,t). \tag{1}$$

These fields are sampled at finite number of points in time. Then, at a fixed time t_n the system displays a snapshot $v_n(x)$, which is a continuous function on Ω. The aim of the POD is to find the most representative structure $\phi(x)$ of the ensemble of N snapshots. This is accomplished by minimizing the objective function (OF) λ:

$$\text{Minimize} \left\{ \lambda = \sum_{n=1}^{N} (\phi(x) - v_n(x))^2 \right\}, \quad \forall x \in \Omega. \tag{2}$$

Equation (2) means that the sum of the differences squared between $v_n(x)$ and $\phi(x)$ should be minimized and can also be written in terms of a maximization problem:

$$\text{Maximize} \left\{ \lambda = \frac{(1/N) \sum_{n=1}^{N} \left(\int_\Omega \phi(x) v_n(x) \, d\Omega \right)^2}{\int_\Omega \phi(x)\phi(x) \, d\Omega} \right\}, \quad \forall x \in \Omega. \tag{3}$$

In order to make the computation unique, we impose the orthonormality condition

$$\int_\Omega \varphi(x)^2 dx = 1. \tag{4}$$

Using the notation

$$(f, g) \equiv \int_\Omega f(x) g(x) \, d\Omega$$

for the inner product of f and g, and

$$\langle v_n \rangle \equiv \frac{1}{N} \sum_{n=1}^{N} v_n(x)$$

for an average of snapshots, it turns out that the ensemble average of the inner products between $v_n(x)$ and $\phi(x)$ must be maximized:

$$\text{Maximize} \left\{ \lambda = \frac{\langle (\phi, v_n)^2 \rangle}{(\phi, \phi)} \right\}, \quad \forall x \in \Omega. \tag{5}$$

The numerator can be expanded to

$$\begin{aligned} \langle (\varphi, v_n)^2 \rangle &= \frac{1}{N} \sum_{n=1}^{N} \left\{ \int_\Omega \varphi(x) v_n(x) \, dx \int_\Omega \varphi(x') v_n(x') \, dx' \right\} \\ &= \int_\Omega \left\{ \int_\Omega \left(\frac{1}{N} \sum_{n=1}^{N} v_n(x) v_n(x') \right) \varphi(x) \, dx \right\} \varphi(x') \, dx'. \end{aligned} \tag{6}$$

The two-point correlation function K is defined as

$$K(x, x') = \frac{1}{N} \sum_{n=1}^{N} v_n(x) v_n(x'). \tag{7}$$

Hence, (6) becomes

$$\langle(\varphi, v_n)^2\rangle = \int_\Omega \left\{ \int_\Omega (K(x,x'))\varphi(x)\,dx \right\} \varphi(x')\,dx'. \tag{8}$$

In view of (8) and (3), the optimization problem can be reduced to the integral eigenvalue problem

$$\int_\Omega (K(x,x'))\phi(x')\,dx' = \lambda\phi(x). \tag{9}$$

Equation (9) has a finite number of orthogonal solutions $\phi_i(x)$, called the POMs with corresponding real and positive eigenvalues λ_i. The eigenvalue with the largest magnitude is the maximum which is achieved in the maximization problem (5). The second largest eigenvalue is the maximum of the same problem restricted to the space orthogonal to the first eigenfunction, and so forth. In order to make the computation unique, the eigenfunctions are normalized. Therefore, the POMs can be used as a basis for the decomposition of the field $v(x,t)$:

$$v(x,t) = \sum_{i=1}^{N} \alpha_i(t)\phi_i(x). \tag{10}$$

Moreover, by construction, the POMs capture more energy than any other modes. It should also be noted that the time-dependent coefficients $\alpha_i(t)$ in Equation (10) are uncorrelated [Azeez and Vakakis 1997].

Thus, the POD can be viewed as a biorthogonal decomposition because of the space/time symmetry of the decomposition. For an accurate approximation of the tensor (7) it is necessary to perform a long and expensive simulation.

2.2. ***Discrete formulation.*** Suppose N linear snapshots $\boldsymbol{v}_i$ of size M obtained for instance by measurements of the acceleration at M locations. The $M \times M$ covariance matrix $\boldsymbol{C}$ is defined as

$$\boldsymbol{C} = \frac{1}{N} \sum_{i=0}^{N-1} \boldsymbol{v_i}\boldsymbol{v}_i^T. \tag{11}$$

Its eigensolutions $(\boldsymbol{\phi}_k, \lambda_k)$, which satisfy

$$\boldsymbol{C}\boldsymbol{\phi}_k = \lambda_k\boldsymbol{\phi}_k, \quad k = 0, \ldots, N-1, \tag{12}$$

with

$$\lambda_0 \geq \lambda_1 \geq \cdots \geq \lambda_{N-1} > 0, \tag{13}$$

characterize the proper orthogonal decomposition. Each eigenvector $\boldsymbol{\phi}_k$ is associated with an eigenvalue λ_k. If the eigenvalues are normalized, they represent the relative energy captured by the corresponding POM. This decomposition is the best basis in terms of decorrelation. The brute computation of the eigensolutions of $\boldsymbol{C}$ is called the *direct method*. However, due to the space-time symmetry property, an alternative method, called the *method of snapshots*, can be employed.

2.3. ***Computation of the POD using SVD.*** The complete biorthogonal decomposition of the data may be obtained by the use of the SVD. Let $x_i(t)$ denote a response time history, where $\boldsymbol{x}$ is a vector containing

the displacement, velocity or acceleration at M discrete locations. We form the discrete matrix

$$\boldsymbol{X} = \begin{bmatrix} x_1(t_1) & \cdots & x_1(t_N) \\ \vdots & \ddots & \vdots \\ x_M(t_1) & \cdots & x_M(t_N) \end{bmatrix}. \tag{14}$$

Thus, each row corresponds to a time history at one location and each column corresponds to a snapshot of the system at a specific time. Now, the singular-value decomposition of matrix $\boldsymbol{X}$ can be written as

$$\boldsymbol{X} = \boldsymbol{U}\,\Sigma\,\boldsymbol{V}^T \tag{15}$$

with $\boldsymbol{U}$ denoting an orthonormal matrix (size $M \times M$) of eigenvectors of $\boldsymbol{X}\boldsymbol{X}^T$ and $\boldsymbol{V}$ an orthonormal matrix (size $N \times N$) of eigenvectors of $\boldsymbol{X}^T\boldsymbol{X}$. The size of the matrix Σ is $M \times N$ but only the main diagonal has non-zero elements which are the singular values of $\boldsymbol{X}$, sorted in descending order. If the matrix $\boldsymbol{X}$ is rank deficient, i.e. some rows (or columns) can be generated by a linear superposition of the others, a few singular values will be zero. The SVD has a lot of applications, e.g. the estimation of the rank of a matrix, the filtering of measurement noise and so forth. In this paper, the aim of the SVD is to compute the POMs and the normalized basic shapes including the response time histories.

3. Basic concepts of morphological processing of one-dimensional functions

Mathematical morphology (MM) was at first introduced as an image-processing method, based on set theory [Serra 1982; Maragos and Schafer 1987]. Since the key element in MM is the set, MM uses nonlinear set processing transformations, starting with two basic operations, Minkowski addition and Minkowski subtraction, based on which a number of morphological operators can be constructed. The basic concept of morphological processing is to use these operators in order to modify the shape of an object, which is considered as a set, by transforming it through its interaction with a second object, called the *structuring element*. The structuring element practically is compact and has a simpler shape compared to the original object.

Limiting for simplicity purposes the application of MM in one-dimensional functions (signals), two different and equivalent approaches in representing functions by sets can be used, in order to apply the set based MM operations.

The first uses the concept of the cross-section of a function, defined as

$$X_t(f) = \{x \in D : f(x) \geq t\}, t \in V, \tag{16}$$

where $f(x)$ is the function under consideration, D is the domain of definition of $f(x)$ over the set Z of integers or the set R of real numbers, V is the range space of $f(x)$, and t is a specified threshold. A graphical presentation of the cross section of a function is shown in Figure 1, left.

Provided practically that the function $f(x)$ is continuous with some possible positive jumps (upper semicontinuous function), then its cross-sections form a sequence of sets which allow the reconstruction of the function as follows [Serra 1982]:

$$f(x) = \sup\{t \in R : x \in X_t\}. \tag{17}$$

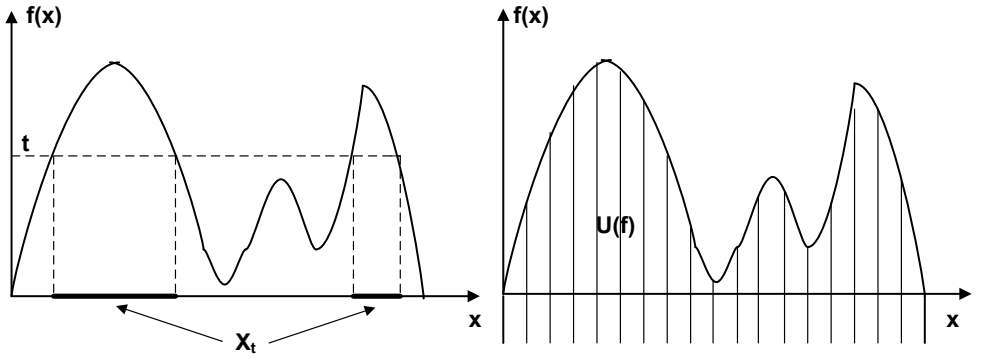

Figure 1. Graphical representation of the cross section $X_t(f)$ and of the umbra $U(f)$ of a function $f(x)$.

The second approach uses the umbra $U(f)$ of the function, represented in Figure 1, right. This is a set U defined in the Cartesian plane by

$$\begin{aligned} U &= \big\{(x,t) : t \le f(x)\big\} = \big\{(x,t) : x \in X_t(f)\big\} \\ &= \big\{(x,t) : w(x,\alpha) \in U,\ \forall \alpha < t\big\}. \end{aligned} \tag{18}$$

The function $f(x)$ can be reconstructed from its umbra:

$$f(x) = \sup\{t \in R : (x,t) \in U(f)\}. \tag{19}$$

Since, according to these definitions, signals can be linked to sets, morphological filtering [Maragos and Schafer 1987] proceeds to the modification of their geometrical characteristics by morphologically processing the signal with another signal or function, called the *structuring element*, which in practice is compact and of a simple shape. Thus a morphological filter is a set mapping operation, which must satisfy four basic requirements: translation invariance, scale invariance, dependence only on the local features of the signal, and upper semicontinuity (meaning that values for arguments near x cannot be far above the value at x, though they can jump down).

Using the equivalent cross-section or umbra representation of a function by sets, Minkowski addition and subtraction between two functions can be defined as

$$(f \oplus g)(x) = \sup_{y \in D}\{f(y) + g(x-y)\}, \qquad (f \ominus g)(x) = \sup_{y \in D}\{f(y) - g(x-y)\}. \tag{20}$$

Here D can be arbitrary, but for practical applications we may assume that D is a compact subset of the real line $\mathbb{R}$ or of the integers $\mathbb{Z}$, containing the support of the function $f(x)$. Using the operations in (20), the four basic morphological operations are defined as

$$\text{Dilation, } \operatorname{dil}(f,g): \quad (f \oplus g^r)(x) = f(x) \oplus g(-x) = \sup_{y \in D}\{f(y) + g(y-x)\}, \tag{21}$$

$$\text{Erosion, } \operatorname{er}(f,g): \quad (f \ominus g^r)(x) = f(x) \ominus g(-x) = \inf_{y \in D}\{f(y) - g(y-x)\}, \tag{22}$$

$$\text{Closing, } \operatorname{cl}(f,g): \quad (f \bullet g)(x) = [(f \oplus g^r) \ominus g](x), \tag{23}$$

$$\text{Opening, } \operatorname{op}(f,g): \quad (f \circ g)(x) = [(f \ominus g^r) \oplus g](x), \tag{24}$$

where $g^r(x)$ denotes the reflected (symmetric) function of $g(x)$ with respect to the origin of the x-axis. These four operations are translation invariant. Opening and dilation are extensive, while erosion and closing are nonextensive operations. Opening and closing are also idempotent operations. For further properties of morphological operations, like distributivity, serial and parallel composition, separability, existence of fixed points, and invertibility, see [Maragos and Schafer 1987].

Compared to the classical linear convolution $f * g$ operation between the two functions $f(x)$ and $g(x)$, the Minkowski addition and subtraction operations of functions can be alternatively defined as nonlinear morphological convolutions, in which the multiplication between the two functions is replaced by summation or subtraction and the summation or integration of the result is replaced by the max or min operations. A similar remark holds for linear correlation, if the reflected function $g^r(x)$ is used, instead of $g(x)$.

However, the nonlinearity of the dilation and the erosion operators results in important differences between these signal operations and the traditional linear convolutions; for instance, serial interconnections of dilations and erosions lead to entirely different nonlinear systems. Thus, there is an infinite variety of nonlinear operators created by cascading dilations and erosions via max, min, addition or subtraction. A thorough treatment of the relations between linear and morphological filtering operations is developed in [Maragos and Schafer 1987], leading to an equivalent representation of the morphological filters above in terms of linear filters. Equations (21)–(24) can be significantly simplified if $g(x)$ is an even function and if sampled functions are used. For a signal $f(k)$, defined over a domain D_f, and for a function $g(u)$ of length L over a domain D_g, called the structuring element, the dilation and the erosion of the signal $f(k)$ by the element $g(u)$ are defined as

$$\mathrm{dil}(k) = (f \oplus g)(k) = \max_{y \in Dg} \{f(k+u) + g(u)\}, \tag{25}$$

$$\mathrm{er}(k) = (f \ominus g)(k) = \min_{u \in Dg} \{f(k+u) - g(u)\}. \tag{26}$$

Similarly, based on erosion and dilation, the closing and the opening operations of the signal $f(k)$ by the element $g(u)$ are further defined as

$$\mathrm{cl}(k) = (f \bullet g)(k) = \mathrm{er}(\mathrm{dil}(k)), \tag{27}$$

$$\mathrm{op}(k) = (f \circ g)(k) = \mathrm{dil}(\mathrm{er}(k)). \tag{28}$$

The geometrical interpretation of these four basic morphological operations for functions can be directly derived by the one used for sets, if the umbra or the cross-section analysis of functions is used. For example, the umbra of the opening is the union of all the translates of the umbra of the structuring element, which can "fit inside" the umbra of the original function.

An example of the application of the four morphological operators to a signal is presented in Figure 2. The erosion of the signal presents a tendency to smooth the abrupt variations of the signal by eliminating the abrupt positive peaks of the signal and enlarging the area around the abrupt negative peaks. The dilation operation leads again to a smoother form of the signal, however this time by "filling" or "dilating" the signal in the areas around the positive peaks. The opening operator eliminates only the positive peaks, while the closing operator eliminates only the negative peaks.

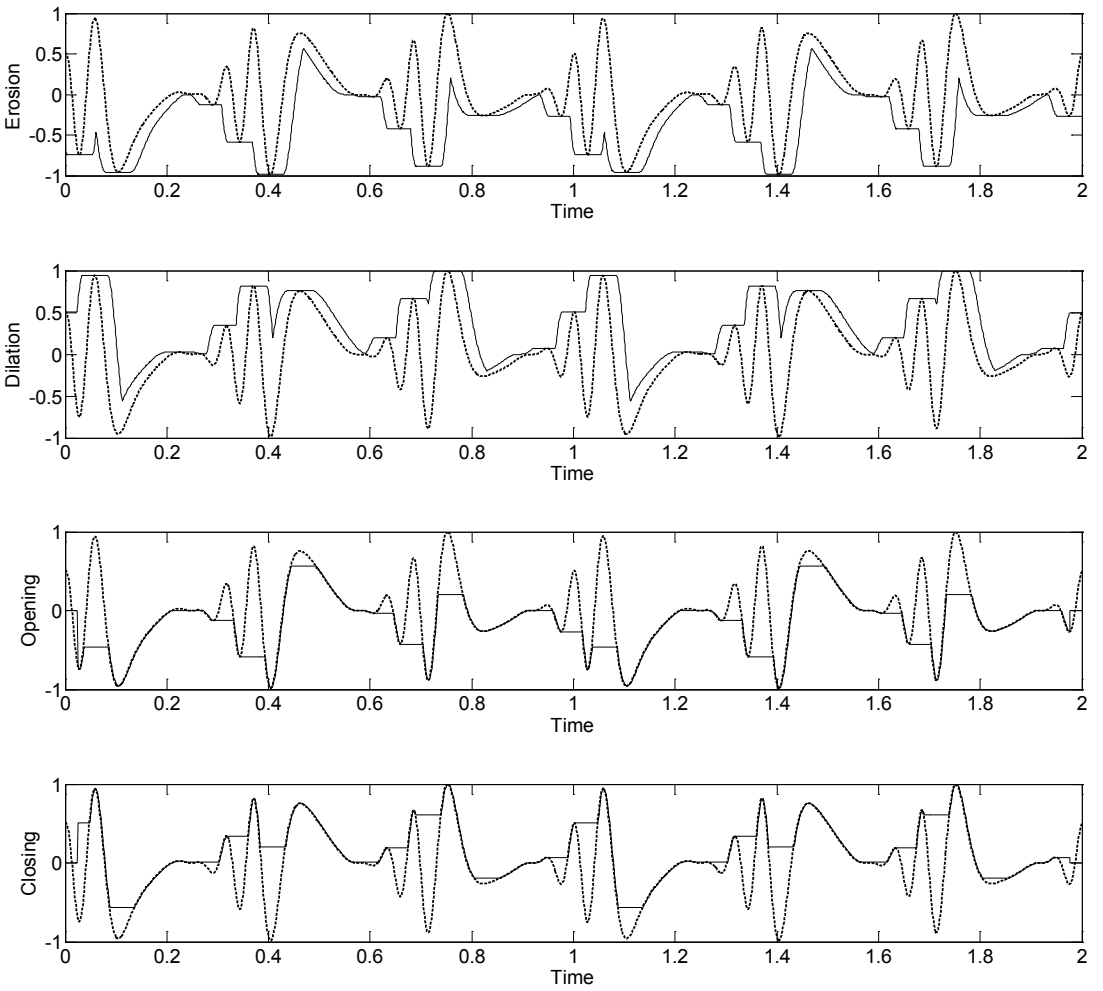

Figure 2. Results of applying the four basic morphological operations to a function (thick dotted line), using a flat structuring element. The thin continuous line is the signal after the operation.

4. Finite element modelling procedure

In order to select an appropriate FEM model to be subsequently used, a comparison is performed between a plane strain 2D model, a plane stress 2D model and a 3D model. The purpose of the analysis is to estimate if the results obtained by an appropriate 2D model can reach the accuracy of a significantly more CPU time consuming 3D model. The analysis includes (I) the healthy structures, (II) an open crack case, (III) a breathing crack case. In the particular case of a breathing crack, contact analysis is performed. All models have been developed in ANSYS 10.0 finite element code.

A clamped cantilever beam of length $l = 300\,\text{mm}$, of uniform square cross-section $w \times w = 20 \times 20\,\text{mm}^2$, with a breathing crack located at $l_c = 150\,\text{mm}$ measured from the clamped end, is considered. The crack has a uniform depth $d = 4\,\text{mm}$ (Relative crack depth $\alpha = d/w = 0.2$ i.e. 20%). The material

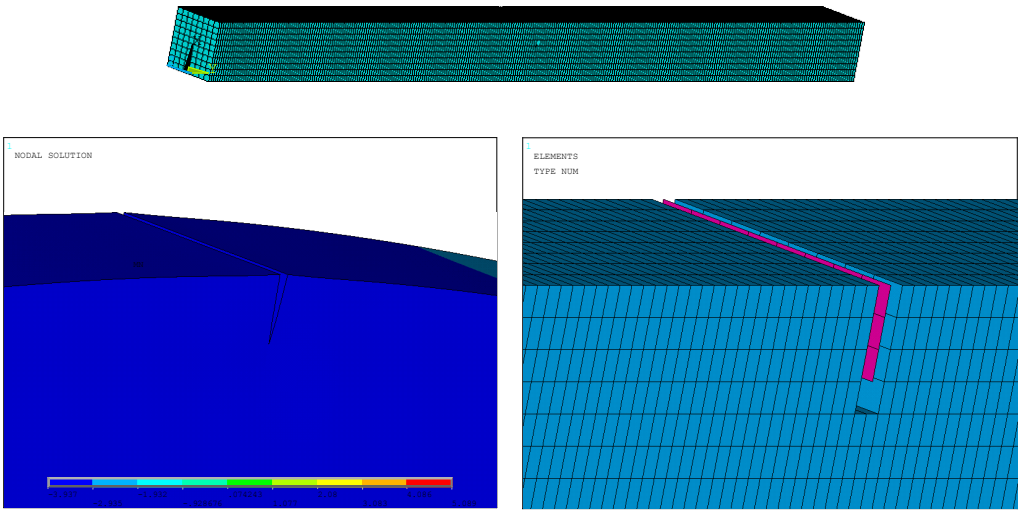

Figure 3. Top: full view of the 3D finite element model. Bottom: zoom of the model in the area of the crack.

properties of a typical Plexiglas material have been considered. The beam is excited by a lateral impact load of 2 MPa uniformly imposed along the vertical free edge, thus causing the crack to open and close.

The finite element mesh consists of 300 subdivisions along the length l and 10 along the other two edges (w) of the cross-section, as shown in Figure 3. The 3D model is built of 8-node solid elements (SOLID45), while on the area of crack surface contact elements were used. The 2D models are built of 4-node elements (PLANE42) in plane stress and plane strain mode. In the case of a breathing crack, line contact elements are used.

First, the natural frequencies for the healthy structure and for the structure with the open crack are calculated. The results are presented in Table 1. As can be noticed, the plane stress model presents an excellent agreement with the 3D model, resulting in less than 0.5% underestimation. On the other hand, the plane strain model results in a natural frequency overestimation of more than 8% with respect to the 3D model. These results do not change essentially when the mesh density is doubled.

In the case of a breathing crack, transient response analysis is performed. The sampling frequency (inverse of the time step) is chosen as 10 KHz and the total time of the analysis as 0.1 s. No damping is

	Beam without crack			Beam with an open crack		
mode	3D	2D plane stress	2D plane strain	3D	2D plane stress	2D plane strain
1st	51.92	51.69	56.49	51.29	51.02	55.75
2nd	318.59	317.22	345.70	303.40	300.89	327.87
3rd	864.20	860.65	934.26	863.94	860.38	933.96

Table 1. Natural frequencies (Hz) of a beam without a crack and for an open crack, as calculated using a three-dimensional, a two-dimensional plane stress and a two-dimensional plane strain finite element model.

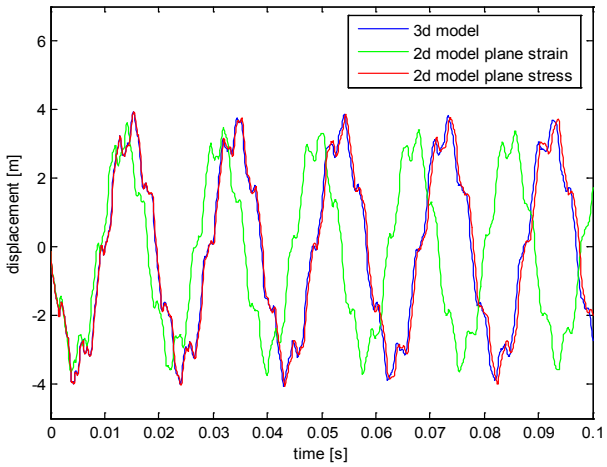

Figure 4. Transverse displacements at the free end of a cantilever beam presenting a breathing crack, using three-dimensional, two-dimensional plane stress and two-dimensional plane strain breathing crack finite element models.

used. The displacement responses over time, as obtained by the three models, are presented in Figure 4. As shown, although the plane stress model has a hardly noticeable difference on the first eigenfrequency than the 3D model, it represents an excellent agreement with the 3D model in terms of displacement amplitude, verifying the corresponding results of Table 1. On the other hand, the plane strain model results in a higher first eigenfrequency and in smaller amplitude compared to the 3D model.

These results show that the 2D plane stress model can be used to reliably describe the case of a beam with a crack, regardless of the type of the crack (open, closed or breathing).

5. Selection of morphological operators and structuring elements

Cracks result in changes of mode shapes, which are much more sensitive to the presence and features of the crack, compared to changes in natural frequencies. However, the presence of damage may not be quite apparent in mode shapes of the lower modes usually measured. For example, the first three POMs are presented in Figure 5 for the cracked beam, described in Section 4.

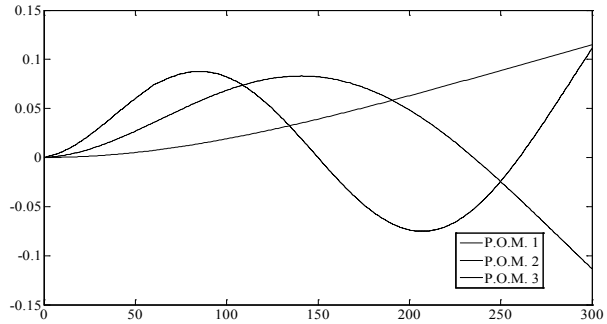

Figure 5. Proper orthogonal modes for the cantilever beam with crack location at 60 mm and relative crack depth 20%.

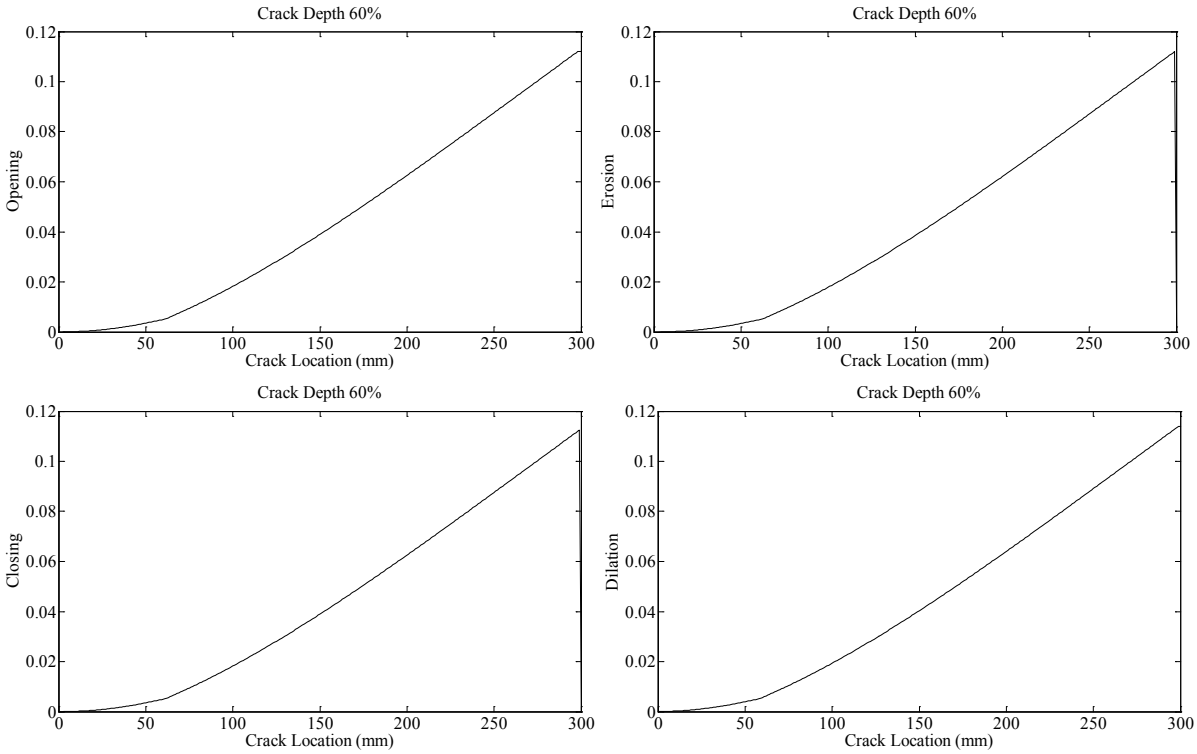

Figure 6. Morphological operators (opening, closing, dilation, erosion) using POM 1 and a flat structuring element.

For this reason, mathematical morphology is further used for processing the shape of the POMs. The effect of each one of the four basic morphological operators of Section 3 (erosion, dilation, opening and closing) are applied on the 3 first POMs in order to examine their ability for better determination of the features of the crack. Furthermore, the choice of a proper structuring element is equally essential for the success of morphological processing.

First a flat structuring element is used. Flat structuring elements are the simplest ones with a straightforward application, since the only parameter to be selected is their corresponding length L. The results can be seen in Figure 6. Although a small change of the slope at the morphological operators can be observed at the location of the crack, this change is not easily identifiable, in order to clearly reveal the existence of the crack.

Then, a spline is used as the structuring element. This spline is created using the corresponding POM of an uncracked beam. The length of the structuring element is selected equal to 1/60 times the length of the beam. The resulting morphological operators are shown in Figure 7. A peak corresponding to the location of the crack is clearly observed at the results of the erosion and of the opening operation, even when the crack is at the first stages (relative crack depth 5%). As a result, both these two morphological operators can be used in principle as crack indicators.

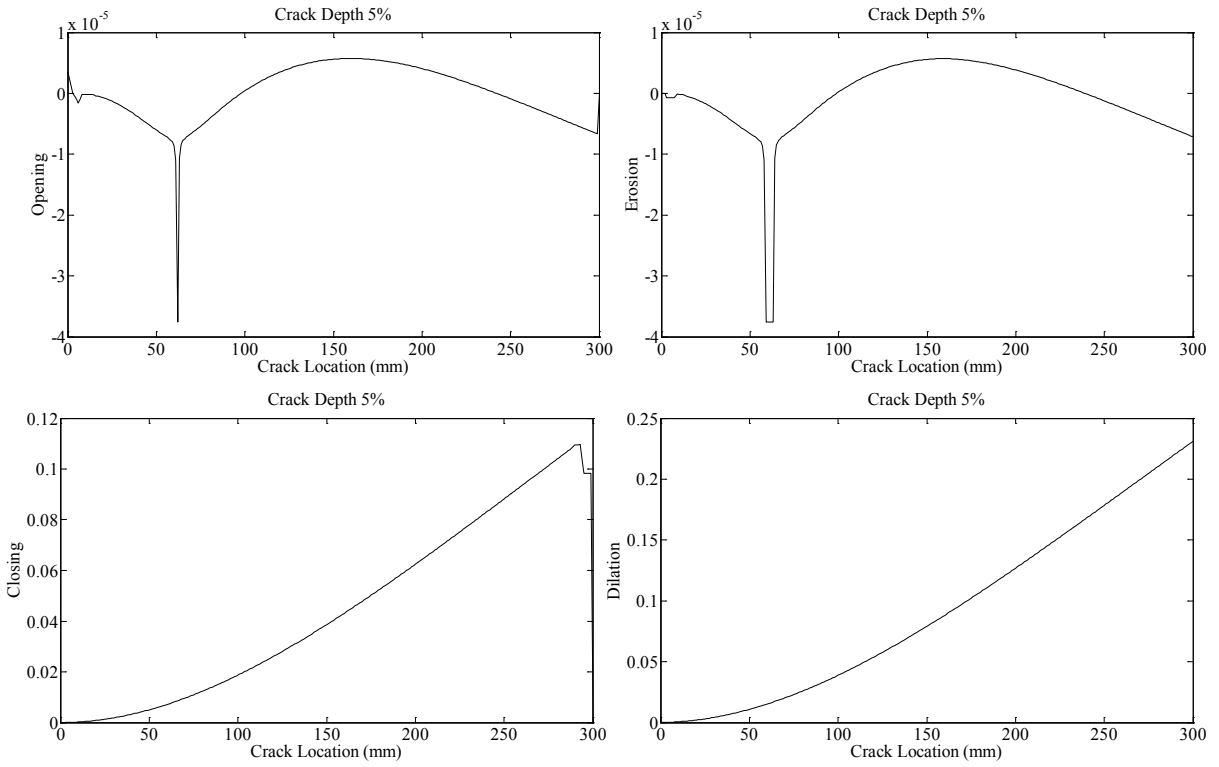

Figure 7. Morphological operators (opening, closing, dilation, erosion) using POM 1 and a spline structuring element, for cantilever beam, crack location at 60 mm, 60% relative crack depth and ANL = 0%.

In the remaining part of the paper, the erosion operator will be used, as it presents a wider peak than opening, a feature which indicates increased robustness. In view of (26) and (28), the opening operator requires more computation time, as its computation involves two steps.

6. Performance assessment in a cantilever beam

In order to assess the efficiency of the proposed approach, its performance with respect to a number of features is been evaluated, such as ability to accurately identify the location and depth of the crack, the identification and the distance of multiple cracks under different depths, the robustness to external noise and the spatial resolution of measurement points.

In the subsequent analysis, the cantilever beam of Section 4 is further processed, using a 2D plane stress model, according to the analysis of Section 4. Single or multiple cracks are introduced each time at distances $l_c = 60$ mm, $l_c = 150$ mm, $l_c = 240$ mm from the clamped end. The relative crack depths α are typically chosen as 10%, 20%, 30%, 40% and 60%. The transverse displacement measurements are obtained at spatial distances of 1 mm along the beam, resulting in a number of $M = 301$ points (spatial locations) available. The erosion operator with a spline structuring element of a length equal to 1/60 of the total beam length is used according to the results in Section 5.

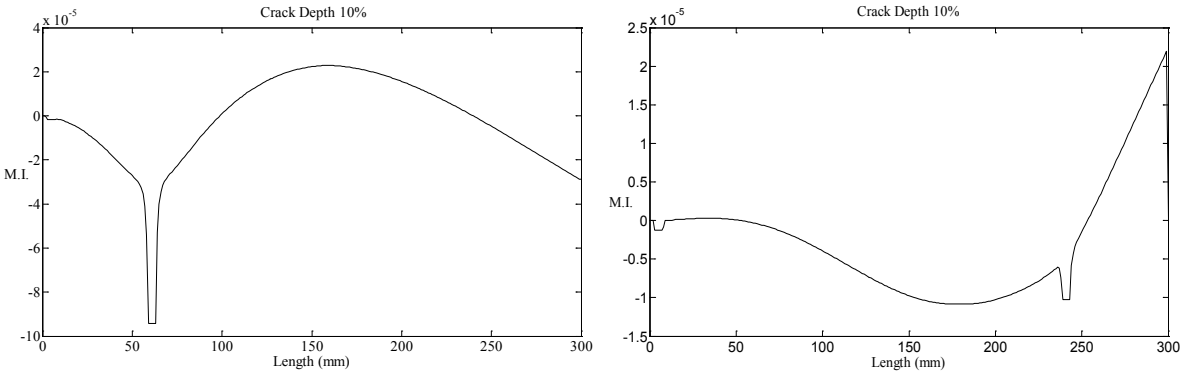

Figure 8. Morphological index using POM 1 with relative crack depth of 10%, ANL = 0%, cantilever beam and crack location at 60 mm (left) or 240 mm (right).

6.1. ***Determination of crack location and depth.*** As already shown in Section 5, the location of the crack can be identified by the sudden change of the erosion morphological operation. The efficiency of this observation is further evaluated under the different crack locations and sizes mentioned above. As seen in Figure 8, the method gives very good results even in the worst case, when the crack is located away from the clamped end at $l_c = 240$ mm and the relative crack depth is only 10%.

In view of this good agreement concerning the crack location, we examine further in Figure 9 the correlation of the evolution of the crack depth with the value of the erosion operator at the crack location. We observe a monotonic increase of the morphological operator with the crack depth. This result can be further exploited in order to use also the value of the morphological operator at the location of the crack as an index (morphological index) to identify the depth of the crack.

However, as seen in Figure 9, left, the results become more clear when the crack is near the middle of the beam. Crack location becomes more difficult when the crack is located near the free ends of the beam.

Contrarily, comparison of just the singular values cannot lead to diagnostic information of the same quality and reliability, as can be observed from Figure 9, right.

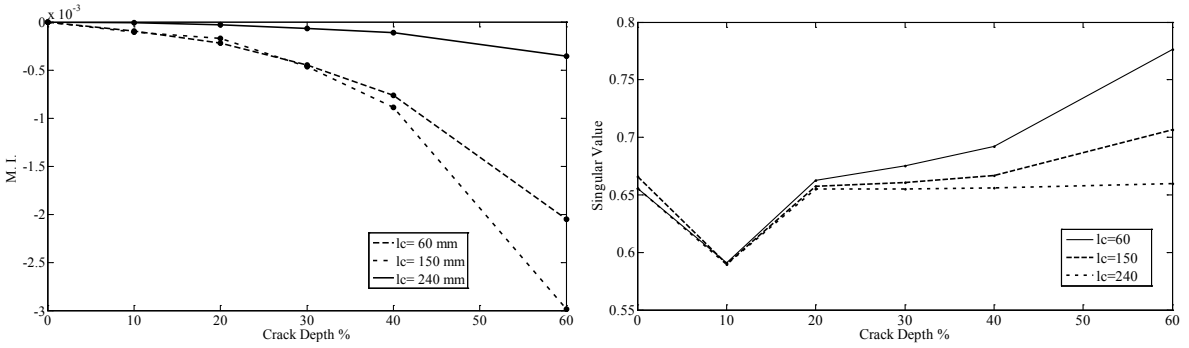

Figure 9. Evolution with crack depth of the morphological index (left) and the first singular value (right) at three locations (ANL = 0%, cantilever beam).

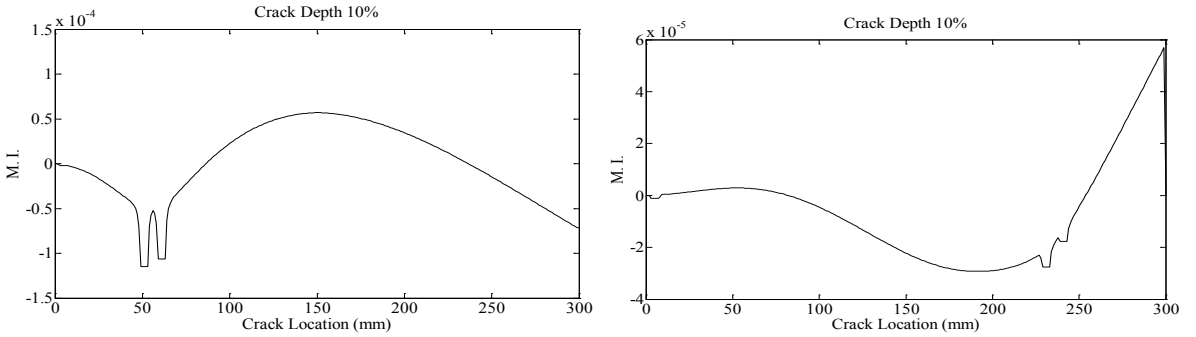

Figure 10. Morphological index using POM 1 with equal relative crack depth of 10%, ANL = 0%, cantilever beam and crack locations at 50 mm and 60 mm (left) or 230 mm and 240 mm (right).

6.2. ***Effects of multiple cracks.*** Two breathing cracks are then simultaneously introduced at different locations of the beam. In view of Figure 10, a peak corresponding to the location of the cracks is again clearly observed, even when the cracks are at the first stage (relative crack depth $\alpha = 10\%$). The method is still able to provide reliable results, even at the worst case when the cracks are located away from the clamped end and closely spaced at $l_{c1} = 230\,\text{mm}$ and $l_{c2} = 240\,\text{mm}$.

6.3. ***Effects of noise.*** In order to examine the effect of noise or measurement errors on the sensitivity of the method, artificial noise was added to the waveforms of the displacements, with an added noise level ANL increased up to a significant amount of 30%. In the case of a single crack, satisfactory results are obtained even for the smallest crack depth of 10% when the crack is located at $l_c = 60\,\text{mm}$ and $l_c = 150\,\text{mm}$ (Figure 11).

In the case of a crack located at $l_c = 240\,\text{mm}$, the detection of the location is easier for big cracks (greater than 40%) and somewhat obscured for smaller ones (less than 30%), as shown in Figure 12. The results become more clear when the third POD is used instead of the first (Figure 13).

However, Figure 14 shows that the worst case, which corresponds to a crack location at $l_c = 240\,\text{mm}$, a relative crack depth of 10% and an ANL of 30%, represents the limits of the detection capability of the method.

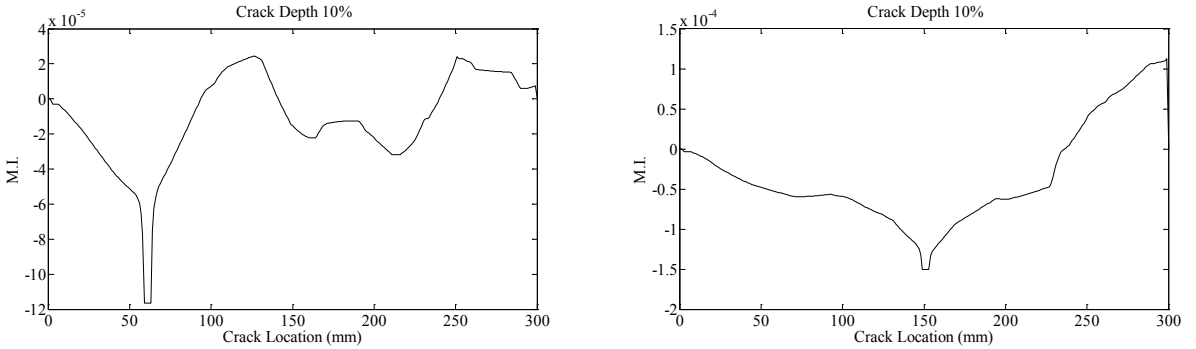

Figure 11. Morphological index using POM 1 with relative crack depth 10%, ANL = 30%, cantilever beam and crack location at 60 mm (left) or 150 mm (right).

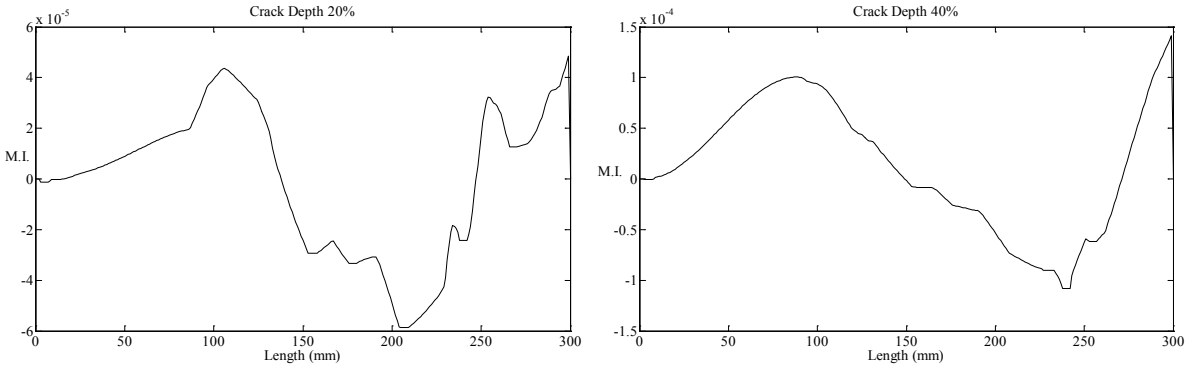

Figure 12. Morphological index using POM 1 with relative crack depth 20% (left) or 40% (right) ANL = 30%, cantilever beam and crack location at 240 mm,

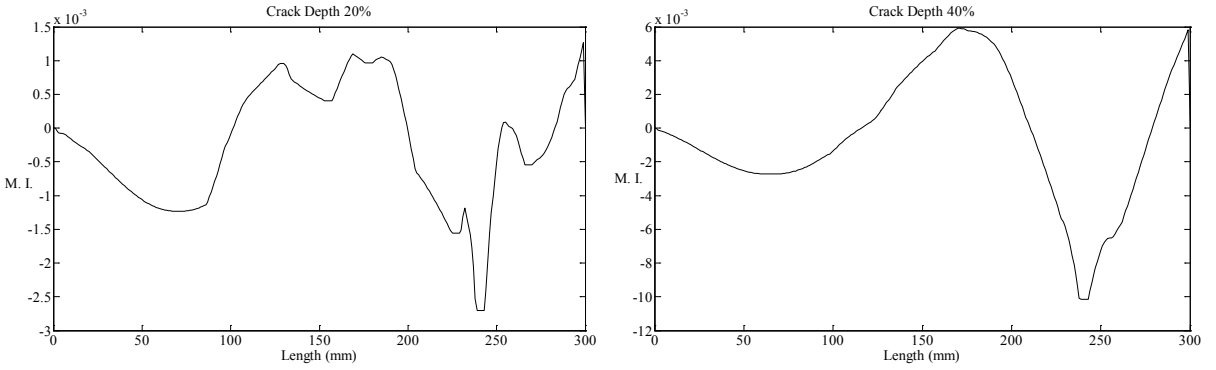

Figure 13. Morphological index using POM 3 for same configuration as in Figure 12.

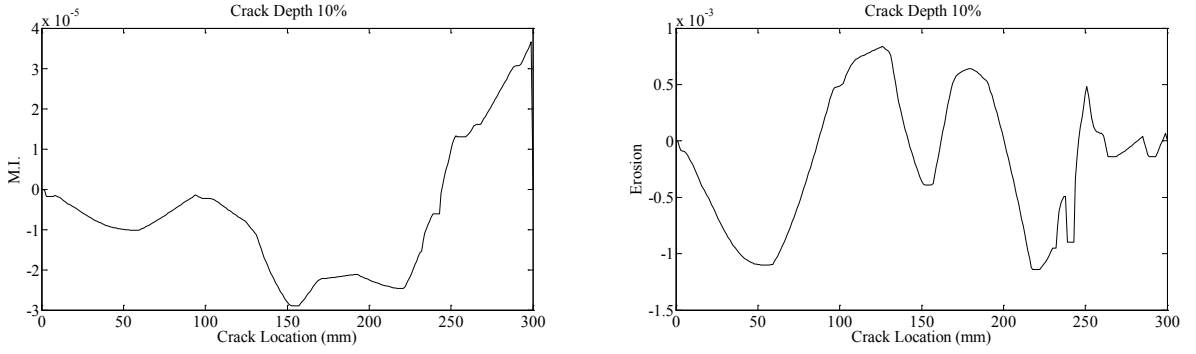

Figure 14. Morphological index using POM 1 (left) or POM 3 (right) with relative crack depth 10%, and ANL = 30%, cantilever beam and crack location at 240 mm.

The evolution of the morphological index with crack depth is presented in Figure 15. Although the method has reached its detection capability limits, the morphological index is still able to follow the increase in crack depth.

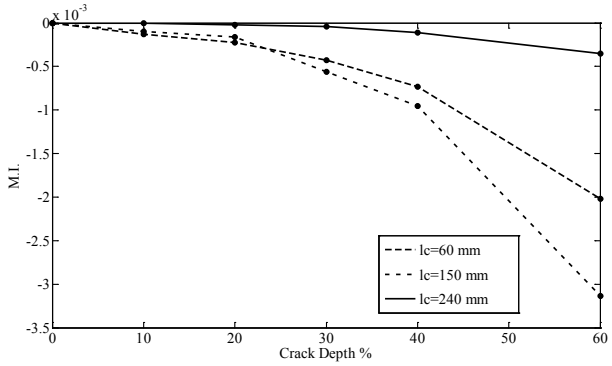

Figure 15. Evolution of the morphological index with crack depth at three locations (ANL=30%, cantilever beam).

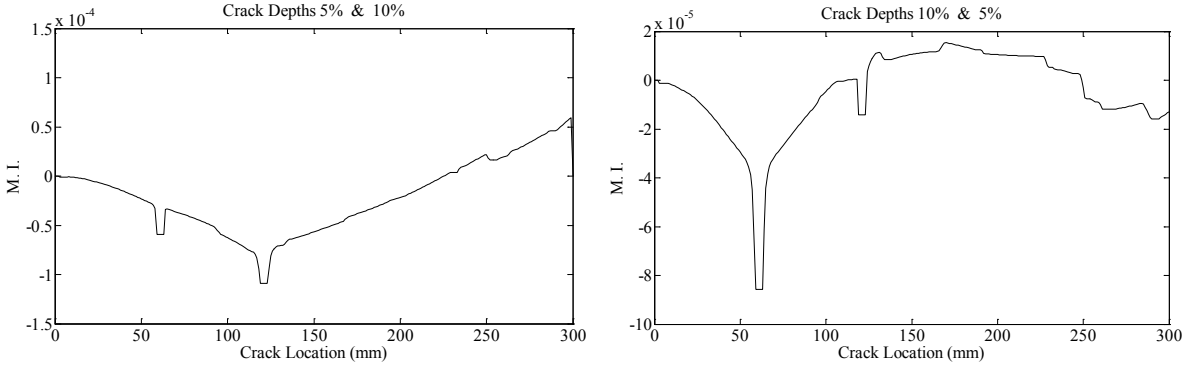

Figure 16. Morphological index using POM 1 with relative crack depths of 5% and 10% (left) or 10% and 5% (right), ANL = 30%, cantilever beam, and crack locations at 60 mm and 120 mm.

In the case of multiple cracks, the crack localization is clear for cracks located at $l_{c1} = 60$ mm, and $l_{c2} = 120$ even at the initial stages of the crack (relative crack depths equal or less than 10%) and for an ANL up to 30% (Figure 16).

The worst case corresponds to crack locations at $l_{c1} = 60$ mm and $l_{c2} = 240$ mm. In the case of an ANL equal to 20%, crack determination is still possible, even when the relative depth of one crack is 10% and of the other is only 5% (Figure 17).

When the ANL increases to 30%, the method reaches again its detection capability limits (Figure 18).

6.4. ***Effect of spatial resolution of measurement points.*** Finally, the effect of decreasing the number of measurement points to the detection capabilities of the method has been evaluated. As a result, in the cases where the two cracks are located far one from each other, the number of the required measurement points can be reduced from $M = 301$ to less than $M = 51$ points, as can be observed in Figure 19. However, as expected, in the cases where the two cracks are close to each other, the method might identify them as a single. This problem can be overcome by increasing the special resolution of the measurement points only locally in the areas of cracks.

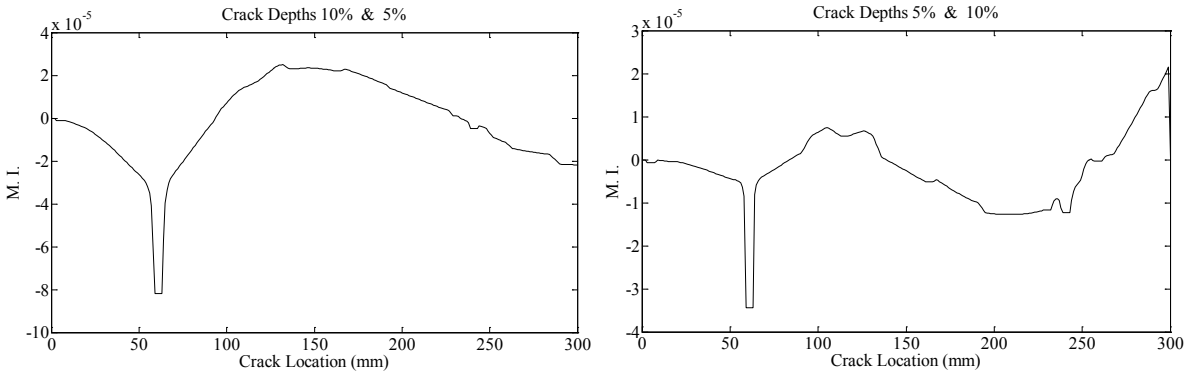

Figure 17. Morphological index using POM 1 with relative crack depths of 10% and 5% (left) or 5% and 10% (right), ANL = 20%, cantilever beam, and crack locations at 60 mm and 240 mm.

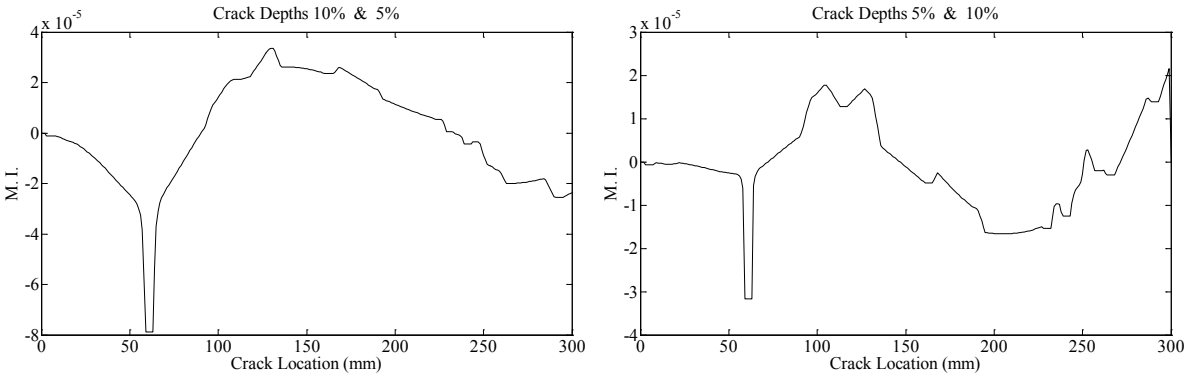

Figure 18. Morphological index using POM 1 with relative crack depths of 10% and 5% (left) or 5% and 10% (right), ANL = 30%, cantilever beam, and crack locations at 60 mm and 240 mm.

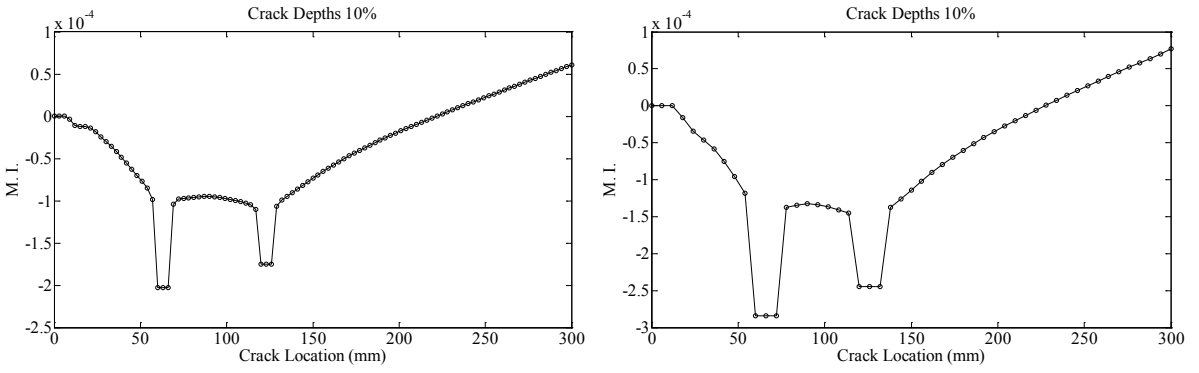

Figure 19. Morphological index using POM 1 with crack locations at 60 mm and 120 mm, equal relative crack depths of 10%, ANL = 0%, cantilever beam, length of the structuring element equal to $L/100$ and number of spatial points M equal to 101 (left) or 51 (right).

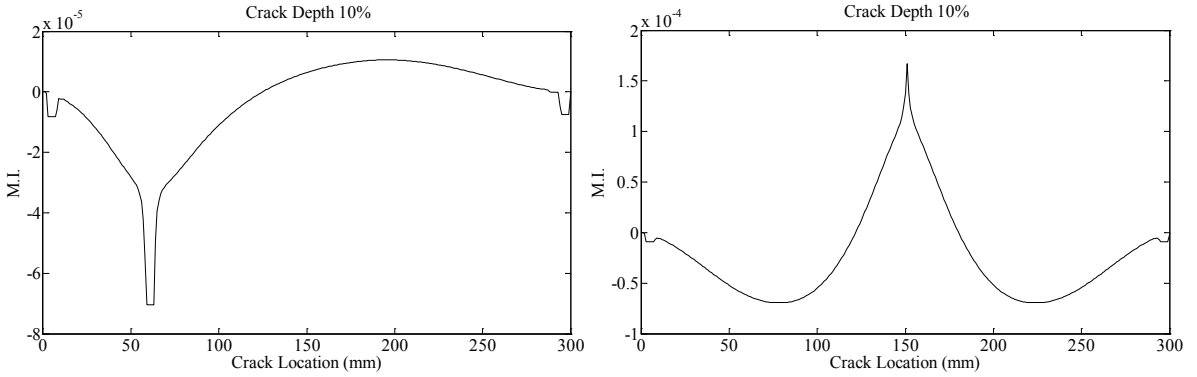

Figure 20. Morphological index using POM 1 with relative crack depth of 10%, ANL = 0%, simply supported beam and crack location at 60 mm (left) or 150 mm (right).

7. Performance assessment in a simply supported beam

The beam of Section 4 is again considered, using a 2D plane stress model, according to the analysis of Section 4. However, this time, the beam is simply supported at both its ends. Single or multiple cracks are introduced each time at distances $l_c = 60$ mm and $l_c = 150$ mm from the beam end. The relative crack depths α are typically chosen as 10%, 20%, 30%, 40%, 50% and 60%. The transverse displacement measurements are obtained at spatial distances of 1 mm along the beam, resulting in a number of $M = 301$ points (spatial locations) available. The erosion operator with a spline structuring element of a length equal to $1/60$ of the total beam length is used according to the results in Section 5.

7.1. ***Determination of crack location and depth.*** As seen in Figure 20, the method gives again very good results even when the relative crack depth is only 10%. Consequently, the evolution of the crack depth with the value of the erosion operator at the crack location is again further examined. As shown in Figure 21, a monotonic increase of the morphological operator is observed with the increase of the crack depth.

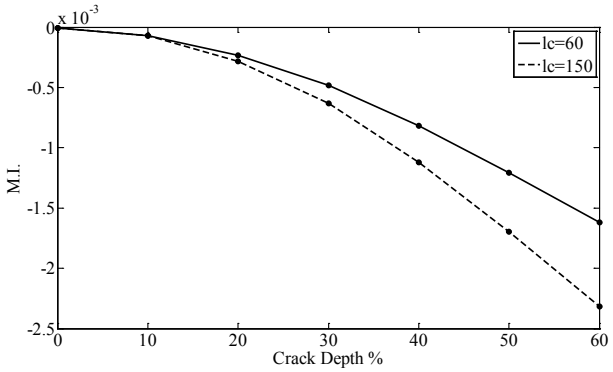

Figure 21. Evolution of morphological index with crack depth at two locations (ANL = 0%, simple beam).

7.2. ***Effects of multiple cracks.*** Two breathing cracks are then simultaneously introduced at different locations of the beam. In Figure 24 on the next page we again observe peaks corresponding to the location of the cracks. These peaks are clearly visible in the case of equal crack depths with relative crack depths as small as 10%. However, in the case of unequal crack depths, the method reaches its limits, with the smaller crack depth being just visible.

7.3. ***Effects of noise.*** In order to examine the effect of noise or measurement errors on the sensitivity of the method, artificial noise was added to the waveforms of the displacements, with an added noise level ANL increased up to a significant amount of 30%. In the case of a single crack, satisfactory results are obtained even for the smallest crack depth of 10%, when the crack is located at the middle of the beam at $l_c = 150$ mm (Figure 22).

In the case of a crack located at $l_c = 60$ mm, the detection of the crack location is easier in case of big cracks (greater than 20%), as shown in Figure 23. However, in view of Figure 22, it is evident that the worst case, which corresponds to a crack location at $l_c = 60$ mm, a relative crack depth of 10% and an ANL of 30%, represents the limits of the detection capability of the method.

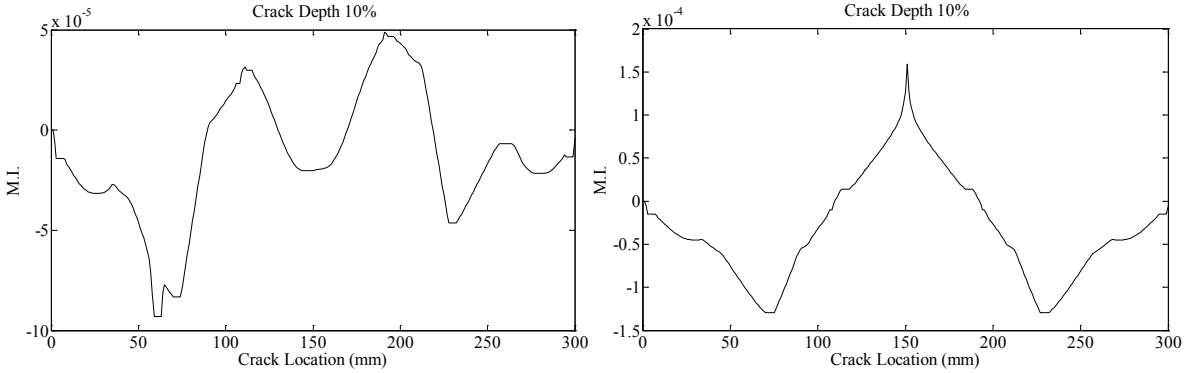

Figure 22. Morphological index using POM 1 with relative crack depth 10%, ANL=30%, simply supported beam and crack location at 60 mm (left) or 150 mm (right).

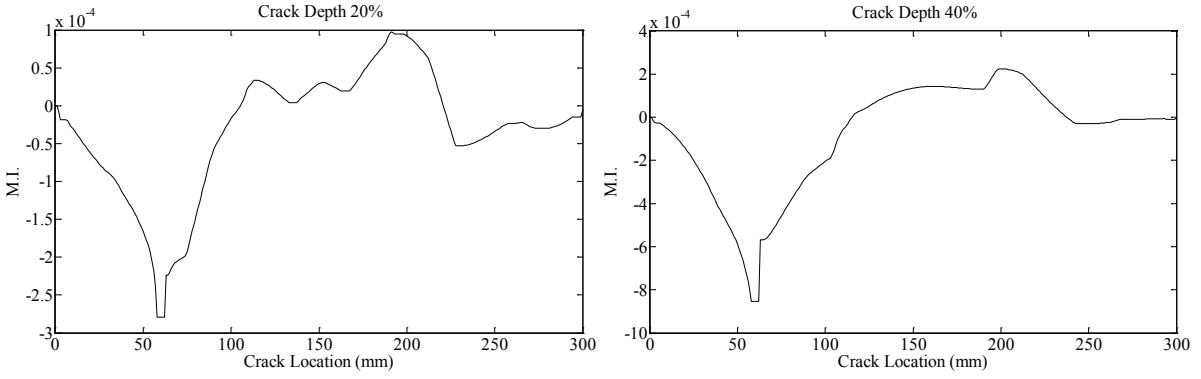

Figure 23. Morphological index using POM 1 with relative crack depth 20% (left) or 40% (right), ANL=30%, simply supported beam and crack location at 60 mm.

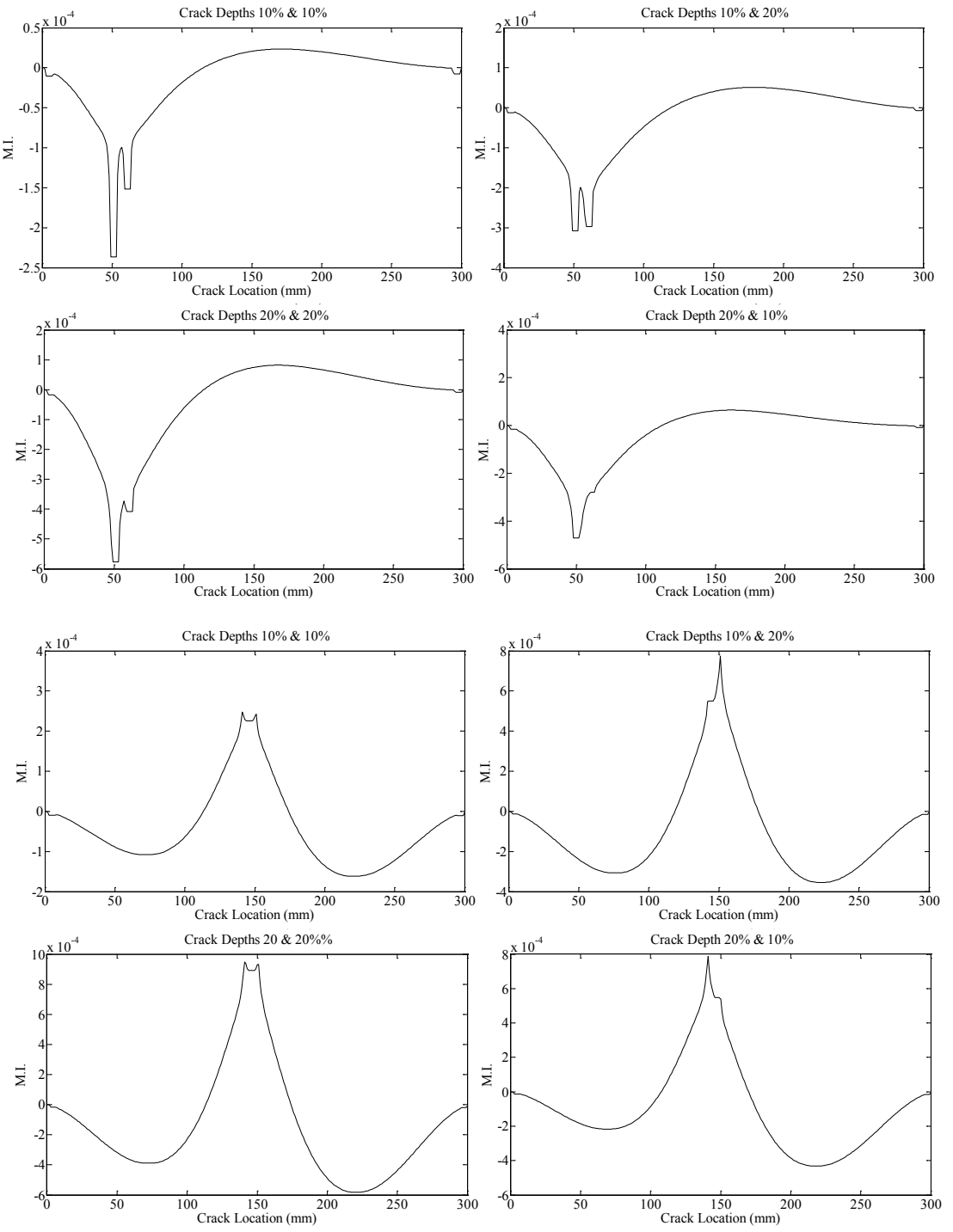

Figure 24. Morphological index using POM 1 for two cracks located at 50 mm and 60 mm (top two rows) or 140 mm and 150 mm (bottom rows), ANL = 0%, simply supported beam, with various relative crack depths.

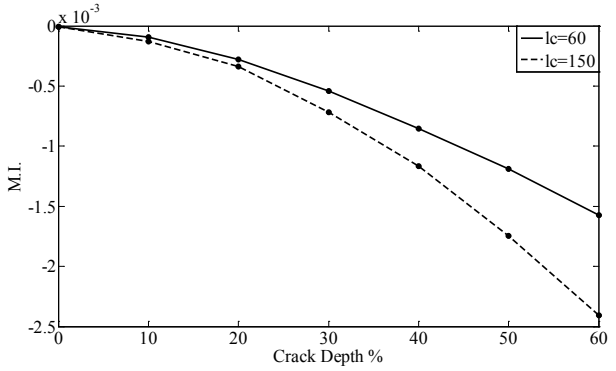

Figure 25. Evolution of the morphological index with crack depth at two locations for (ANL=30%, simply supported beam).

The evolution of the morphological index with crack depth is shown in Figure 25. Although the method has reached its detection capability limits, the morphological index is still able to follow the increase of the depth of the crack.

In the case of multiple cracks, Figure 27 on the next page suggests that the effect of noise is marginal, compared to the effect of unequal cracks (Section 7.2).

7.4. ***Effect of spatial resolution of measurement points.*** Finally, the effect of decreasing the number of measurement points to the detection capabilities of the method is again evaluated, for a crack located at $l_c = 60$ mm. In view of Figure 26, the number of the required measurement points can be reduced from $M = 301$ to less than $M = 51$ points. However, as again expected, in the cases where the two cracks are close to each other, the method might identify them as a single. This problem can be overcome by increasing the spatial resolution of the measurement points only locally in the areas of cracks.

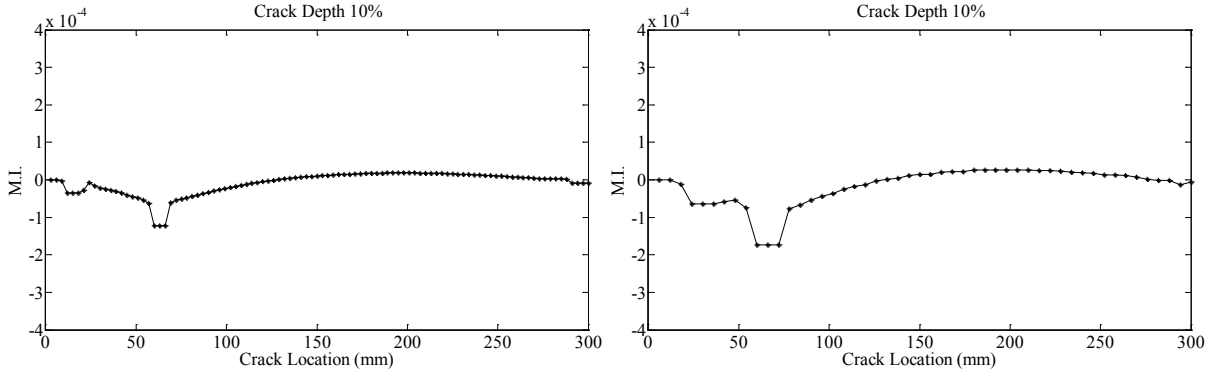

Figure 26. Morphological index using P.O.M. 1 with crack location at 60 mm for relative crack depth of 10%, ANL = 0%, simply supported beam, length of the structuring element equal to $L/100$ and number of spatial points used as A) $M = 101$ points (Left), B) $M = 51$ points (Right)

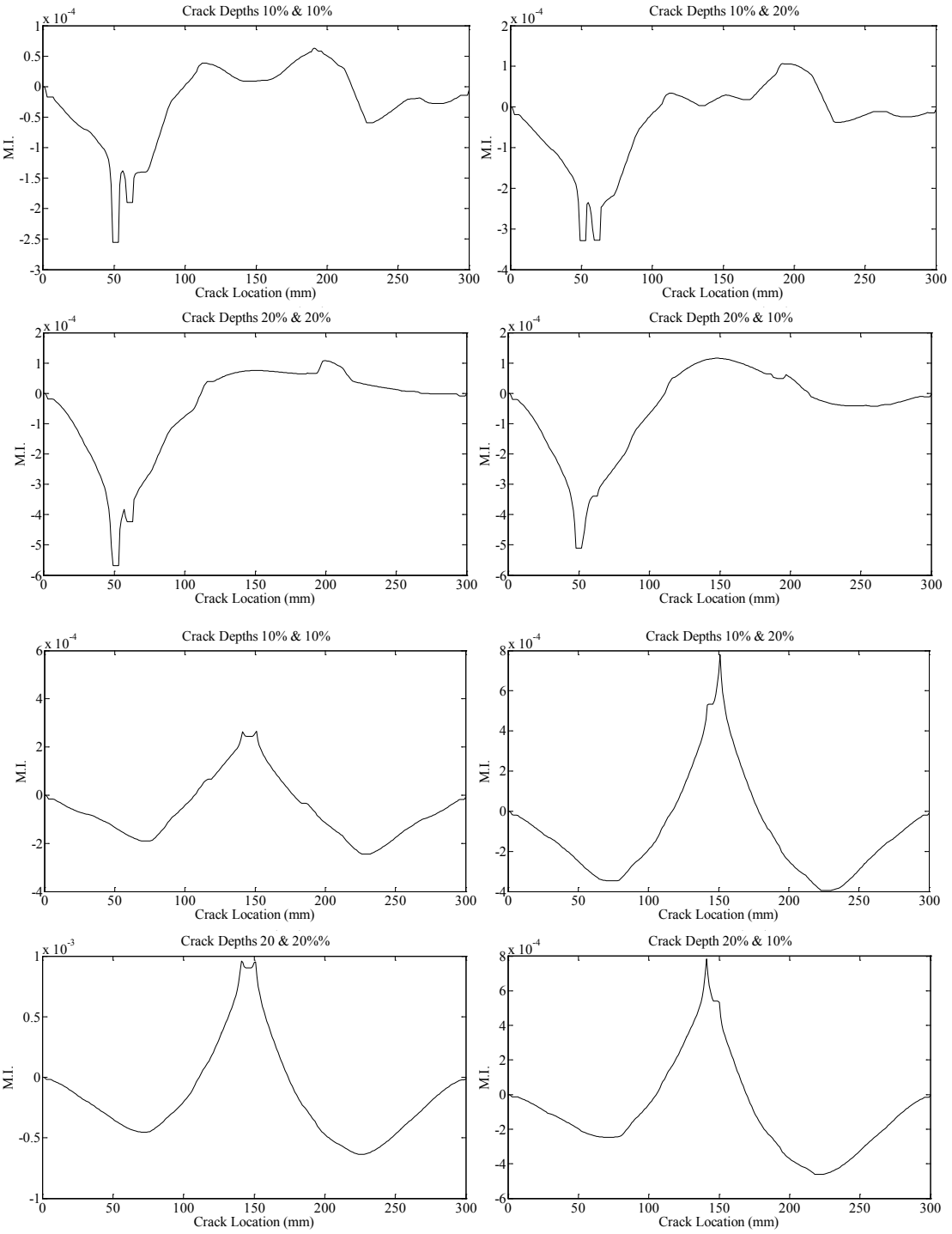

Figure 27. Morphological index using POM 1 for two cracks located at 50 mm and 60 mm (top two rows) or 140 mm and 150 mm (bottom rows), ANL = 30%, simply supported beam, with various relative crack depths.

8. Conclusion

A comparison of different FEM models (2D plane stress, 2D plane strain, 3D) used to model a cantilever beam with a crack indicates that the 2D plane stress model can accurately and reliably model the crack effect, whether if the crack is of open, closed or breathing type. From the four basic morphological operators (erosion, dilation, opening, and closing) used to process the proper orthogonal modes of the cracked beam, the erosion operator using a spline structuring element presents the best behavior.

The proposed method, as assessed both in a cantilever and in a simply supported beam, can lead to the efficient detection both of the crack location, as well as of the crack size. Due to the fact that POMs are used instead of modes, nonlinear effects can be taken into account and noise effects can be eliminated. The morphological index can follow the evolution of the crack depth, even when the signal to noise ratio reaches 30%. The results become clearer when more than one POM is used. In the case of double-cracked beam structures, the analysis of the effect of different crack depths, noise level and spatial resolution of the measured points indicate that the proposed method can present also robust results.

Acknowledgements

This work is cofunded by the European Social Fund (75%) and National Resources (25%) - Operational Program for Educational and Vocational Training II (EPEAEK II) and particularly the Program PYTHAGORAS.

References

[Alvandi and Cremona 2006] A. Alvandi and C. Cremona, "Assessment of vibration-based damage identification techniques", *J. Sound Vib.* **292**:1–2 (2006), 179–202.

[Andreaus et al. 2007] U. Andreaus, P. Casini, and F. Vestroni, "Non-linear dynamics of a cracked cantilever beam under harmonic excitation", *Int. J. Non-Linear Mech.* **42**:3 (2007), 566–575.

[Azeez and Vakakis 1997] M. F. Azeez and A. F. Vakakis, "Numerical and experimental analysis of the nonlinear dynamics due to impacts of a continuous overhung rotor", in *Proceedings of the 1997 ASME Design Engineering Technical Conferences* (*DETC97*) (Sacramento, CA, 1997), edited by B. Ravani, ASME, New York, 1997.

[Bamnios et al. 2002] Y. Bamnios, E. Douka, and A. Trochidis, "Crack identification in beam structures using mechanical impedance", *J. Sound Vib.* **256**:2 (2002), 287–297.

[Cawley 1997] P. Cawley, "Long range inspection of structures using low frequency ultrasound", pp. 1–17 in *Structural damage assessment using advanced signal processing procedures: proceedings of DAMAS '97* (Sheffield, 1997), edited by J. M. Dulieu-Smith et al., Sheffield Academic Press, Sheffield, 1997.

[Cawley and Adams 1979] P. Cawley and R. D. Adams, "The location of defects in structures from measurements of natural frequencies", *J. Strain Anal. Eng. Des.* **14**:2 (1979), 49–57.

[Chang and Chen 2005] C.-C. Chang and L.-W. Chen, "Detection of the location and size of cracks in the multiple cracked beam by spatial wavelet based approach", *Mech. Syst. Signal Process.* **19**:1 (2005), 139–155.

[Cheng et al. 1999] S. M. Cheng, X. J. Wu, W. Wallace, and A. S. J. Swamidas, "Vibrational response of a beam with a breathing crack", *J. Sound Vib.* **225**:1 (1999), 201–208.

[Dimarogonas 1996] A. D. Dimarogonas, "Vibration of cracked structures: a state of the art review", *Eng. Fract. Mech.* **55**:5 (1996), 831–857.

[Doebling et al. 1998] S. W. Doebling, C. R. Farrar, and M. B. Prime, "A summary review of vibration-based damage identification methods", *Shock Vib. Digest* **30**:2 (1998), 91–105.

[Douka and Hadjileontiadis 2005] E. Douka and L. J. Hadjileontiadis, "Time-frequency analysis of the free vibration response of a beam with a breathing crack", *NDT&E Int.* **38**:1 (2005), 3–10.

[Douka et al. 2003] E. Douka, S. Loutridis, and A. Trochidis, "Crack identification in beams using wavelet analysis", *Int. J. Solids Struct.* **40**:13–14 (2003), 3557–3569.

[Douka et al. 2004] E. Douka, S. Loutridis, and A. Trochidis, "Crack identification in plates using wavelet analysis", *J. Sound Vib.* **270**:1–2 (2004), 279–295.

[Farrar et al. 1994] C. R. Farrar, W. E. Baker, T. M. Bell, K. M. Cone, T. W. Darling, T. A. Duffey, A. Eklund, and A. Migliori, "Dynamic characterization and damage detection in the I-40 bridge over the Rio Grande", Technical Report LA-12767-MS, Los Alamos National Laboratory, Los Alamos, NM, 1994.

[Feeny 1997] B. F. Feeny, "Interpreting proper orthogonal modes in vibrations", in *Proceedings of the 1997 ASME Design Engineering Technical Conferences* (*DETC97*) (Sacramento, CA, 1997), edited by B. Ravani, ASME, New York, 1997.

[Galvanetto and Violaris 2007] U. Galvanetto and G. Violaris, "Numerical investigation of a new damage detection method based on proper orthogonal decomposition", *Mech. Syst. Signal Process.* **21**:3 (2007), 1346–1361.

[Guo and Billings 2007] L. Z. Guo and S. A. Billings, "Detection of fatigue cracks in a beam using a spatio-temporal dynamical system identification method", *J. Sound Vib.* **299**:1–2 (2007), 22–35.

[Hadjileontiadis et al. 2005a] L. J. Hadjileontiadis, E. Douka, and A. Trochidis, "Crack detection in beams using kurtosis", *Comput. Struct.* **83**:12–13 (2005), 909–919.

[Hadjileontiadis et al. 2005b] L. J. Hadjileontiadis, E. Douka, and A. Trochidis, "Fractal dimension analysis for crack identification in beam structures", *Mech. Syst. Signal Process.* **19**:3 (2005), 659–674.

[Kim et al. 2003] J.-T. Kim, Y.-S. Ryu, H.-M. Cho, and N. Stubbs, "Damage identification in beam-type structures: frequency-based method vs mode-shape-based method", *Eng. Struct.* **25**:1 (2003), 57–67.

[Lenaerts et al. 2001] V. Lenaerts, G. Kerschen, and J. C. Golinval, "Proper orthogonal decomposition for model updating of non-linear mechanical systems", *Mech. Syst. Signal Process.* **15**:1 (2001), 31–43.

[Lifshitz and Rotem 1969] J. M. Lifshitz and A. Rotem, "Determination of reinforcement unbonding of composites by a vibration technique", *J. Compos. Mater.* **3**:3 (1969), 412–423.

[Loutridis et al. 2004] S. Loutridis, E. Douka, and A. Trochidis, "Crack identification in double-cracked beams using wavelet analysis", *J. Sound Vib.* **277**:4–5 (2004), 1025–1039.

[Loutridis et al. 2005] S. Loutridis, E. Douka, L. J. Hadjileontiadis, and A. Trochidis, "A two-dimensional wavelet transform for detection of cracks in plates", *Eng. Struct.* **27**:9 (2005), 1327–1338.

[Lumley 1967] J. L. Lumley, "The structure of inhomogeneous turbulent flows", pp. 166–178 in *Atmospheric Turbulence and Radio Wave Propagation*, edited by A. M. Yaglom and V. I. Tatarski, Nauka, Moscow, 1967.

[Luzzato 2003] E. Luzzato, "Approximate computation of non-linear effects in a vibrating cracked beam", *J. Sound Vib.* **265**:4 (2003), 745–763.

[Maragos and Schafer 1987] P. Maragos and R. Schafer, "Morphological filters, I: Their set-theoretic analysis and relations to linear shift-invariant filters", *IEEE Trans. Acoust. Speech Signal Process.* **35**:8 (1987), 1153–1169.

[Ostachowicz and Krawczuk 1991] W. M. Ostachowicz and M. Krawczuk, "Analysis of the effect of cracks on the natural frequencies of a cantilever beam", *J. Sound Vib.* **150**:2 (1991), 191–201.

[Randall 2002] R. B. Randall, "State of the art in monitoring rotating machinery", pp. 1457–1477 in *Noise and vibration engineering: proceedings of ISMA 2002* (Leuven, 2002), vol. 4, edited by P. Sas and B. van Hal, Katholieke Universiteit Leuven, Department of Mechanical Engineering, Leuven, 2002.

[Ruotolo and Surace 1997] R. Ruotolo and C. Surace, "Damage assessment of multiple cracked beams: numerical results and experimental validation", *J. Sound Vib.* **206**:4 (1997), 567–588.

[Rytter 1993] A. Rytter, *Vibration based inspection of civil engineering structures*, Ph.D. thesis, Aalborg University, Aalborg, 1993.

[Sahin and Shenoi 2003] M. Sahin and R. A. Shenoi, "Quantification and localisation of damage in beam-like structures by using artificial neural networks with experimental validation", *Eng. Struct.* **25**:14 (2003), 1785–1802.

[Sekhar 2008] A. S. Sekhar, "Multiple cracks effects and identification", *Mech. Syst. Signal Process.* **22**:4 (2008), 845–878.

[Serra 1982] J. Serra, *Image analysis and mathematical morphology*, Academic Press, New York, 1982.

[Sohn et al. 2004] H. Sohn, C. R. Farrar, F. M. Hemez, D. D. Shunk, D. W. Stinemates, B. R. Nadler, and J. J. Czarnecki, "A review of structural health monitoring literature: 1996–2001", Technical Report LA-13976-MS, Los Alamos National Laboratory, Los Alamos, NM, 2004, Available at http://institute.lanl.gov/ei/shm/pubs/LA_13976_MSa.pdf.

[Wang and Deng 1999] Q. Wang and X. Deng, "Damage detection with spatial wavelets", *Int. J. Solids Struct.* **36**:23 (1999), 3443–3468.

[Zhong and Oyadiji 2007] S. Zhong and S. O. Oyadiji, "Crack detection in simply supported beams without baseline modal parameters by stationary wavelet transform", *Mech. Syst. Signal Process.* **21**:4 (2007), 1853–1884.

Received 18 Nov 2008. Revised 4 Jun 2009. Accepted 4 Jun 2009.

KONSTANTINOS C. GRYLLIAS: kosgryl@central.ntua.gr
National Technical University of Athens, School of Mechanical Engineering, Heroon Polytechniou 9, 15780 Athens, Greece

IOANNIS N. KOUKOULIS: jkouk@central.ntua.gr
National Technical University of Athens, School of Mechanical Engineering, Heroon Polytechniou 9, 15780 Athens, Greece

CHRISTOS T. YIAKOPOULOS: chryiako@central.ntua.gr
National Technical University of Athens, School of Mechanical Engineering, Heroon Polytechniou 9, 15780 Athens, Greece

IOANNIS A. ANTONIADIS: antogian@central.ntua.gr
National Technical University of Athens, School of Mechanical Engineering, Heroon Polytechniou 9, 15780 Athens, Greece

CHRISTOPHER G. PROVATIDIS: cprovat@central.ntua.gr
National Technical University of Athens, School of Mechanical Engineering, Heroon Polytechniou 9, 15780 Athens, Greece
http://users.ntua.gr/cprovat/